Patterning SS304 Surface at Microscale to Reduce Wettability and Corrosion in Saline Water

Vivek Anand Annakodi, Ramachandra Arvind Singh, Subramanian Jayalakshmi, Yupeng Zhang, Muhammed Anaz Khan, Koppula Srinivas Rao, Rajashekhara Shabadi

metals

MDPI

Article

Patterning SS304 Surface at Microscale to Reduce Wettability and Corrosion in Saline Water

Vivek Anand Annakodi [1], Ramachandra Arvind Singh [2,*], Subramanian Jayalakshmi [2,*], Yupeng Zhang [3], Muhammed Anaz Khan [4], Koppula Srinivas Rao [5] and Rajashekhara Shabadi [6,*]

[1] Department of Aeronautical Engineering, MLR Institute of Technology, Hyderabad 500043, India; vivekanandbit@gmail.com
[2] School of Mechanical and Electrical Engineering, Wenzhou University, Wenzhou 325035, China
[3] College of Materials and Fujian Key Laboratory of Materials Genome, Xiamen University, Xiamen 361005, China; ypzhang25@gmail.com
[4] Department of Mechanical Engineering, MLR Institute of Technology, Hyderabad 500043, India; muhammedanazkhan@gmail.com
[5] Department of Computer Science and Engineering, MLR Institute of Technology, Hyderabad 500043, India; ksreenu2k@gmail.com
[6] UMR 8207-UMET-Unité Matériaux et Transformations, University Lille, CNRS, INRAE, Centrale Lille, F-59000 Lille, France
* Correspondence: r.arvindsingh@gmail.com (R.A.S.); jayalakshmi.subramanian@gmail.com (S.J.); rajshekhara.shabadi@univ-lille.fr (R.S.)

Abstract: Stainless steel 304 (SS304) experiences corrosion when it is exposed to a saline atmosphere, which attains severity due to its high surface wettability. Topographical modification of metallic surfaces is an effective route to reduce wettability and thereby mitigate liquid-mediated corrosion. In this work, topographical modification of stainless steel 304 flat surface in the form of micropillars was done (pillar width: 100 μm, inter-pillar distance: 100 μm and height: 80 μm). Micropillars were fabricated by a chemical etching process. Wetting and corrosion of the micropillars was studied over long-time duration in comparison with flat surface, before and after intermittent and continuous exposures to saline water for 168 h. Wetting was characterized by measuring the static water contact angle on the test surfaces and their corrosion by electrochemical polarization tests (electrolyte: 3.5 wt.% sodium chloride solution). The relationship between the nature of wetting of the test surfaces and their corrosion was examined. Micropillars showed predominantly composite wetting over a long time, which imparted an effective resistance against corrosion over a long time to the SS304 surface. When compared to the flat surface, the corrosion rates of the micropillars were lower by two orders of magnitude, prior to and also upon long-time contact with the NaCl solution. Micropillars lowered corrosion due to composite wetting, i.e., solid-liquid-air interface that reduced the area that was in contact with the NaCl solution. The efficiency of corrosion inhibition (η) of micropillars was 88% before long-time contact, 84% after intermittent contact, and 77% after continuous contact with NaCl solution. Topographical modification in the form of micropillars that can impart composite wetting is an effective route to induce long-term anticorrosion ability to the SS304 surface.

Keywords: 304 stainless steel; micropillars; wettability; corrosion; saline water

Citation: Annakodi, V.A.; Arvind Singh, R.; Jayalakshmi, S.; Zhang, Y.; Anaz Khan, M.; Srinivas Rao, K.; Shabadi, R. Patterning SS304 Surface at Microscale to Reduce Wettability and Corrosion in Saline Water. *Metals* **2022**, *12*, 1137. https://doi.org/10.3390/met12071137

Academic Editors: Francesca Borgioli and Hannu Hänninen

Received: 9 May 2022
Accepted: 29 June 2022
Published: 3 July 2022

1. Introduction

Micropatterning of metallic surfaces is an effective route to lower liquid-mediated corrosion [1]. Micropatterns can offer efficiency of corrosion inhibition that is comparable to those that are obtained by chemical modification of metallic surfaces [1]. Micropatterns have several advantages over conventional approaches that mitigate corrosion such as thin films/coatings, electroplating, paints, and inhibitors, e.g., absence of interface between surface and corrosive media, devoid of complex chemical processes, easy to design and fabricate patterns of varying geometries (i.e., shape/size), multifunctionality (e.g., drag

reduction, antifouling, anti-frosting/icing, and antifriction [2–4]). The advantages of micropatterning of surfaces, in detail, are given in [1].

Metallic micropatterns that have been reported to effectively reduce liquid-mediated corrosion include: microcell structures that are fabricated on aluminum surfaces by laser direct writing technique [5], patterns of micro-holes that are generated by laser ablation on nickel surfaces [6], micro-holes that are created on 316LVM stainless steel wires by focused ion beam (FIB) method [7], textures on SS316L that are produced by Nd:YAG nanosecond laser [8], chemically-etched microchannels on 304 stainless steel surfaces [9], and laser-textured and heat-treated aluminum 7075 alloy [10]. However, these studies [5–10] report one-time testing of corrosion of micropatterns. Recent work on hydrophobic SS304 microgrooves reports that micropatterning provides long-term antiwetting and long-term anticorrosion abilities [1]. Long-term examination of wetting and corrosion of micropatterns is important as it provides insights for application purposes. Using additive manufacturing technology, metallic parts with micropatterns can be fabricated in one-step. Figure 1 shows micropillars on a copper part printed in a single step by FluidFM 3DP method [11]. Additive manufacturing of micropatterns having anticorrosion capabilities can be easily realized on metallic surfaces without resorting to post-manufacturing machining/processing.

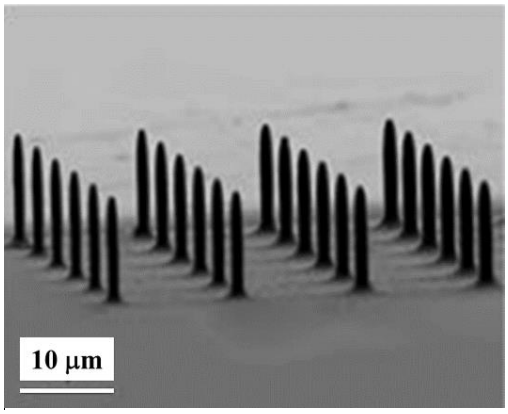

Figure 1. Micropillars on a copper part printed in a single step by FluidFM 3DP method [11].

Stainless steel 304 (SS304) has application in structures/architecture, food processing, biomedical, automobile, and aerospace industries [12]. SS304 is resistant to chemicals due to the presence of chromium element. However, it is prone to corrosion in salt-water due to the presence of aggressive chloride ions [13,14]. High surface wettability of the steel aggravates salt-water corrosion [1,13,14]. Hence, by reducing the surface wettability of the steel, its corrosion by salt-water can be reduced. Consequently, its performance can be enhanced in humid/marine environments. Micropatterning of metallic surfaces for anticorrosion functionality can be easily realized due to flexibility in the geometrical design of micropatterns that can impart composite wetting. Hydrophobic SS304 microgrooves, anisotropic in their geometry and wetting nature have shown long-term anticorrosion ability against saline water [1]. In this work, micropatterns in the form of micropillars, isotropic in their geometry and wetting nature, fabricated on SS304 flat surfaces were examined for their long-time wettability characteristics and corrosion response over a long time, when exposed to saline water. The objective was to identify the effectiveness of micropillar topography on SS304 to reduce corrosion in saline water, over long-time duration.

2. Materials and Methods

As-received SS304 steel surfaces were polished using emery sheets (grit size: 80, 120, 220, 400, 600, 1000, and 2000). Subsequently, the surfaces were subjected to diamond polishing. The polished surfaces were cleaned with acetone. Using a 3D optical profilometer (WYKO NT1100, Champaign, IL, USA), the roughness of the surfaces was measured. The

average surface roughness (Ra) of the polished surfaces was 0.015 µm. These surfaces were taken as the reference surface and are referred to as flat surface. The flat surface and topographically-modified flat surface in the form of micropillars were taken as the test surfaces. Data on the wettability and corrosion behaviour of SS304 flat surface is referred from [1].

2.1. SS304 Micropillar Surfaces

Square shaped micropillars (MP) were fabricated on SS304 flat surfaces by chemical etching. MP was fabricated by PCM Crafts Pvt Ltd., Bengaluru, India [9]. In the first step, the cleaning of SS304 flat surfaces was conducted using acetone, followed by distilled water, and subsequently dried (Figure 2a). Next, a photoresist was coated on the flat surfaces via spin coating at the speed of 500 rpm, at 25 °C with a stay time of 30 s. A square micropattern design was engraved on the photoresist using a laser (Figure 2b). An etchant solution of ferric chloride mixed with water in equal proportion was prepared and was kept for 2 h to stabilize. Hydrofluoric acid was added to the prepared solution in the ratio of 1:10. Subsequently, the flat surfaces with their photomasks were dipped in the etchant solution (Figure 2c). Areas on the flat surfaces that were not covered by photomasks got chemically etched, leaving behind micropillars on top of the flat surfaces (Figure 2d). The fabricated MP was thoroughly cleaned with acetic acid mixed with deionized water in the proportion of 1:10, to remove photoresist that was sticking on the surface (Figure 2e).

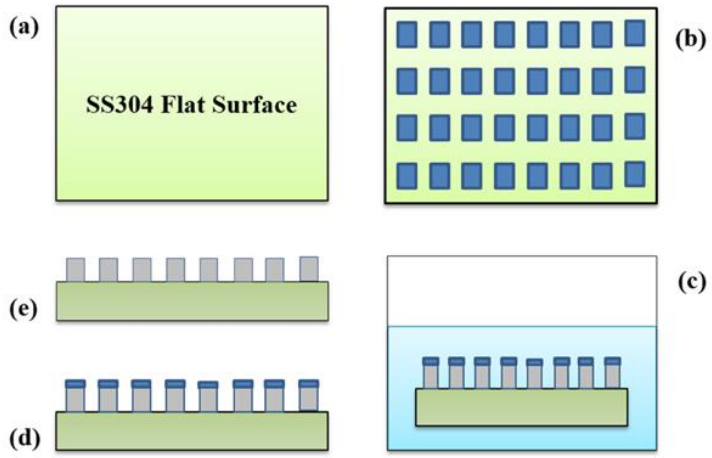

Figure 2. Fabrication of micropillars on SS304 flat surface using a chemical etching method. (**a**) SS304 flat surface, (**b**) square micropattern design engraved on the photoresist coated on the flat surface, (**c**) flat surface with photomask dipped in an etchant solution, (**d**) micropillars on top of the flat surface, and (**e**) micropillars upon removal of photomask.

An image of MP that was taken by an optical 3D profilometer (WYKO NT1100, Champaign, IL, USA) is shown in Figure 3a. The spatial distribution of micropillars (unit cell) and geometrical parameters of MP, namely pillar width ($W_p \approx 100$ µm), inter-pillar distance ($D_p \approx 100$ µm), and pillar height ($H_p \approx 80$ µm) are shown as schematics in Figure 3b,c. A scanning electron microscope (SEM) image of MP that was taken after fabrication is shown in Figure 3d and an optical microscope image is shown in Figure 3e. Using the optical profilometer, the roughness (Ra) was measured on top of the surfaces of the micropillars. The average value of the surface roughness (Ra) was 0.018 µm.

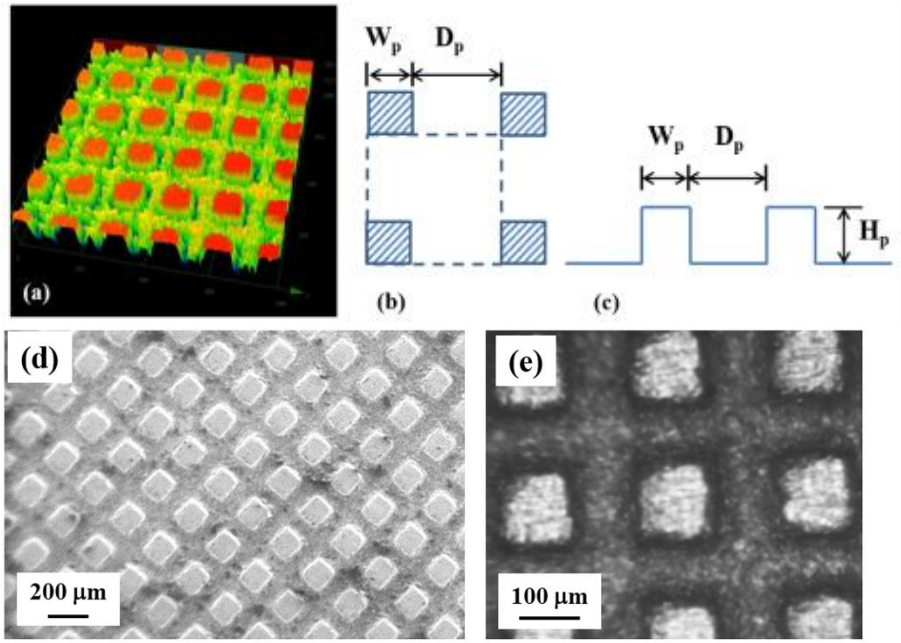

Figure 3. (**a**) Image of micropillar surface (MP) taken by a 3D optical profilometer. (**b**) Spatial distribution of micropillars on the flat surface (unit cell). (**c**) Geometrical parameters of MP: pillar width ($W_p \approx 100$ µm), inter-pillar distance ($D_p \approx 100$ µm) and pillar height ($H_p \approx 80$ µm). (**d**) SEM image of MP taken after fabrication. (**e**) Optical microscope image of MP.

2.2. Wettability Test

The wettability test was conducted by measuring the static water contact angle (CA) on the flat and MP surface. Before each measurement, using acetone and distilled water, the test surfaces were cleaned and subsequently dried. Measurements were conducted using a contact angle goniometer (Data Physics OCA15EC, Filderstadt, Germany), by placing water droplets (distilled water, droplet volume 5 µL) on the test surfaces. CA values reported are averages from ten measurements (error $\pm$ 2°).

2.3. Electrochemical Polarization Test

Potentiodynamic polarization tests were conducted with saline water as the electrolyte (3.5 wt.% NaCl solution), using an electrochemical workstation (Autolab, Metrohm, The Netherlands). Working electrodes were the test surfaces, reference electrodes were Ag/AgCl, and the counter electrode was platinum. Prior to testing, the test surfaces were dipped in saline water (contact area 1 cm^2) for 60 min to attain steady state open circuit potential. Subsequently, corrosion tests were conducted and polarization curves were recorded (scan rate: 1 mV/s; potential range for each test surface was $\pm$0.1 V relative to its open circuit potential [1]). From the curves, the corrosion potential (E_{corr}) and corrosion current density (i_{corr}) were determined. Using Stern–Geary relation [15], the corrosion rates were estimated.

2.4. Long-Time Exposures to NaCl Solution

Long-time exposure to NaCl solution was conducted under two conditions:

(i) Intermittent exposure: saline water droplets were dispensed on the test surfaces (kept inclined at 45°, industrial weathering tests [16]) at the rate of 1 droplet/s, using a droplet generator, for 168 h.
(ii) Continuous exposure: flat and MP samples were immersed in saline water for the duration of 168 h, separately.

The CA was measured at the interval of every 24 h for 168 h. Before measuring CA, the test samples were subjected to drying in an open atmosphere for 30 min [1].

A corrosion test of the flat surface and MP was conducted before and after long-time exposures to 3.5 wt.% NaCl solution (i.e., saline water). Before conducting the corrosion test, all test samples (i.e., those subjected to long-time exposures and that which was not exposed) were cleaned with acetone and dried in open atmosphere for 15 min. The test samples namely, flat surface and MP were characterized for their wetting and corrosion behavior on one sample for each test condition, respectively (i.e., prior to, intermittent, continuous exposures to NaCl solution). The CA values that are reported are averages from ten measurements. The surfaces that were used to measure contact angles, were subsequently subjected to corrosion test (one test was conducted for each condition of exposure to NaCl solution).

3. Results & Discussion

3.1. Wetting Behaviour

Chemical modifications of metallic surfaces prevented contact with corrosive fluids and thus acts as a barrier to chemicals, e.g., thin films, coatings, electroplating, paints, etc. Contrarily, in topographically-modified surfaces, e.g., micropatterned surfaces, the surfaces remain in contact with corrosive fluids, and hence their wettability directly influences their corrosion. The contact angle of water drop (CA) on a surface is an indicator of the wettability of the surface.

The measured CA value of the flat surface and MP as a function of exposure time to NaCl solution (t), for intermittent exposure and continuous exposure, are shown in Figure 4a,b, respectively. Figure 4 also shows representative pictures of the water droplets on the test surfaces, taken before and after long-time exposures to NaCl solution. The CA values of the flat surface and MP, measured prior to (0 h), and after intermittent contact and continuous contact with NaCl solution (168 h) are given in Table 1.

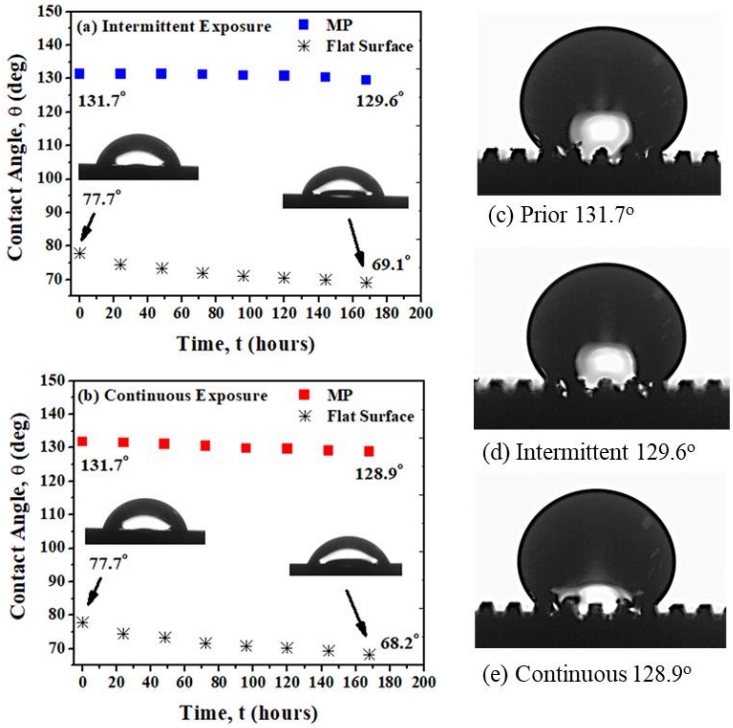

Figure 4. Measured contact angle value (CA) of the flat surface and MP as a function of exposure time to the NaCl solution (t ≈ 168 h): (**a**) intermittent exposure and (**b**) continuous exposure. Insets in (**a**,**b**) show images of water droplets on the flat surface, taken before and after long-time contacts with NaCl solution, in the corresponding conditions of exposure. Images of water droplets on micropillar surface (MP): (**c**) before long-time exposure, (**d**) after intermittent exposure and (**e**) after continuous exposure to NaCl solution.

Table 1. Water contact angles (CA) of the flat surface [1] and micropillar surface (MP) prior to and (I) after intermittent contact and (II) after continuous contact with NaCl solution. θ_r values (θ_r = contact angle prior to long-time exposure—contact angle after long-time exposure) of the flat surface [1] and MP: (I) after intermittent contact and (II) after continuous contact with NaCl solution.

Surface	Contact Angle (°)			θ_r (°)	
	Prior to Long-Time Contacts	I	II	I	II
Flat	77.7	69.1	68.2	8.6	9.5
MP	131.7	129.6	128.9	2.1	2.8

Wetting of water droplets on micropatterned surfaces is usually explained by two classical theoretical models, the Wenzel model and the Cassie–Baxter model [17]. According to these models: (i) water droplet in the Wenzel state, due to solid-liquid interface, wets the top of surface features and the area between them, i.e., complete wetting, and (ii) water droplet in Cassie–Baxter state, due to solid-liquid-air interface, wets the top of surface features, with air trapped in between the surface features, i.e., composite wetting. There exists a critical angle of transition from the Wenzel state to Cassie–Baxter state (θ_C), above which a water droplet on a micropatterned surface attains Cassie–Baxter state. θ_C can be theoretically estimated for micropillars, as given by Equation (1) [18].

$$\text{Cos } \theta_C = (f - 1)/(r - f) \quad (1)$$

where, θ_C is the critical angle, r is the roughness parameter (ratio of the actual total surface area and planar surface area), and f is the solid fraction (ratio of the actual wetted surface area and planar surface area). Roughness parameter (r) for square shaped micropillars can be estimated by using Equation (2) [19].

$$r = 1 + 4\,(W_p H_p)/P^2 \quad (2)$$

where, W_p is the micropillar width, H_p is the micropillar height, and P is the pitch (distance between the centers of two adjacent micropillars). The solid fraction (f) for square shaped micropillars is given by $W_p{}^2/P^2$ [19]. In the present case, for MP: W_p is 100 μm, H_p is 80 μm and P is 200 μm. The roughness parameter (r) is 1.8, solid fraction (f) is 0.25, and θ_C is 118.9°. The measured CA vales of MP are higher than the estimated θ_C value (Table 1). The Cassie–Baxter contact angle (θ_{CB}) can be theoretically estimated using Equation (3) [19].

$$\text{Cos } \theta_{CB} = f\,(\text{Cos } \theta + 1) - 1 \quad (3)$$

where, θ is the contact angle of the flat surface. For the MP surface, the estimated θ_{CB} before long-time exposures, after intermittent exposure, and continuous exposure are 134.1°, 131.3°, and 131°, respectively. The measured CA values of MP (Table 1) are slightly lower than those that were estimated theoretically (θ_{CB}). Theoretical estimation considers perfect geometry, i.e., square shaped micropillars with sharp edges. However, in the present case, most of the micropillars do not have sharp edges rather they have round edges (Figure 3), which is due to the fabrication process, i.e., chemical etching. Sharp edges strongly pin water droplets, and so CA have larger values [20]. Thus, having round edged micropillars, MP shows CA values that are lower than those that are estimated theoretically (θ_{CB}). Taken together, the results indicate that water droplets on MP experience composite wetting, with some wetting of micropillars over their sides, owing to their round edges.

The CA values of the flat surface prior to, and after intermittent contact and continuous contact with NaCl solution are <90° (Table 1) indicating that the flat surface is hydrophilic. The CA values of the test surfaces decrease with the increase in the exposure time (t). A reduction in CA for the test surfaces due to long-term exposures (θ_r = contact angle prior to long-time exposure—contact angle after long-time exposure), is given in Table 1.

When compared to the θ_r values of the flat surface, the θ_r values of MP are 4-times lower for intermittent exposure, and 3.4-times lower for continuous exposure. Upon long-time exposures, the flat surface experiences rapid increase in wettability, indicated by its higher θ_r values. MP has long-term antiwetting ability as indicated by its lower θ_r values.

3.2. Corrosion Behaviour

Corrosion parameters (E_{corr}, i_{corr}, and corrosion rate, CR) of the flat surface [1] and MP, before and after long-time contacts with NaCl solution are given in Tables 2 and 3, respectively. Figure 5 shows Tafel plots of the test surfaces.

Table 2. Corrosion potential (E_{corr}), corrosion current density (i_{corr}), and corrosion rate (CR) of the flat surface [1] and micropillar surface (MP) before long-time contacts with NaCl solution.

Surface	Before Long-Time Contacts		
	E_{corr} (V)	i_{corr} (A/cm^2)	CR (mm/Year)
Flat Surface	−0.5121	11.16×10^{-6}	166×10^{-4}
MP	−0.0217	1.35×10^{-8}	1.01×10^{-4}

Table 3. Corrosion parameters (E_{corr}, i_{corr}, and corrosion rate, CR) of the flat surface and micropillar surface [1] (MP) after long-time contacts with NaCl solution.

Surface	After Intermittent Contact			After Continuous Contact		
	E_{corr} (V)	i_{corr} (A/cm^2)	CR (mm/Year)	E_{corr} (V)	i_{corr} (A/cm^2)	CR (mm/Year)
Flat Surface	−0.2703	26.6×10^{-6}	311×10^{-4}	−0.2789	26.9×10^{-6}	313×10^{-4}
MP	−0.0249	1.76×10^{-8}	1.31×10^{-4}	−0.0273	2.57×10^{-8}	1.82×10^{-4}

Compared to the flat surface, MP has (i) higher values of E_{corr}, (ii) lower values of i_{corr}, and (iii) lower CR values (lower in magnitude by two orders). Considering the CA values (Table 1) and the CR values (Tables 2 and 3) of the test surfaces, it is seen that as the CA values decrease, the CR values increase. In magnitude, CA values of the test surfaces have the trend such that the values before long-time contact > after intermittent contact > after continuous contact. The CR values of the test surfaces have the trend such that the magnitude before long-time contact < after intermittent contact < after continuous contact. These results indicate that the wettability of the test surfaces influences their corrosion. After long-time contacts with NaCl solution, the CA values of test surfaces decrease due to capillarity that is caused by the formation of pits [1]. In comparison to the flat surface, MP has higher CA values and, therefore, lower CR values, at all the test conditions. The CA values of MP reduced by 1.6% and 2.12% after intermittent contact and continuous contact, respectively. The CR values of MP showed 29.7% and 80.19% increase when compared to the CR value before long-time contacts, respectively. The CA values of the flat surface decreased by 11% and 12.2% after intermittent contact and continuous contact, respectively [1]. The CR values of flat surface showed 87.3% and 88.5% increase when compared to the CR value before long-time contacts, respectively [1]. Dependence of CR on CA, as observed in the present work, has been reported for other metallic patterns [1,5,7–9].

Microscopic images of surfaces of MP taken after corrosion tests are shown in Figure 6. The corrosion products that dislodged from the top region of micropillars are seen at the bottom in the vicinity of micropillars. This is more evident from the images that were taken at higher magnification (yellow arrows, Figure 6d,e). From these two figures, it is also seen that some wetting of micropillars has occurred over their sides that are adjacent to the top (shown by red arrows), which is due to their round edges. These observations reveal that wetting by the fluid occurs predominantly in a composite state, while it also wets the sides of micropillars near their top region, and that the fluid has not come in contact with the bottom area in between the micropillars. These observations corroborate

the wetting and corrosion test results. Based on the observation that some wetting occurs at the sides of micropillars, it can be inferred that the solid fraction (f) of MP will be >0.25 (theoretically estimated value), but remains <1 (f is 1 for flat surface). Due to smaller area that comes in contact with the corrosive fluid, MP has CR values that are significantly lower than those of the flat surface. Surface wetting directly depends on area that is in contact with a fluid [1,21–23]. Under composite wetting conditions, air that is trapped in between micropillars prevents entry of corrosive fluid and electrochemical activity [1,5,8–10].

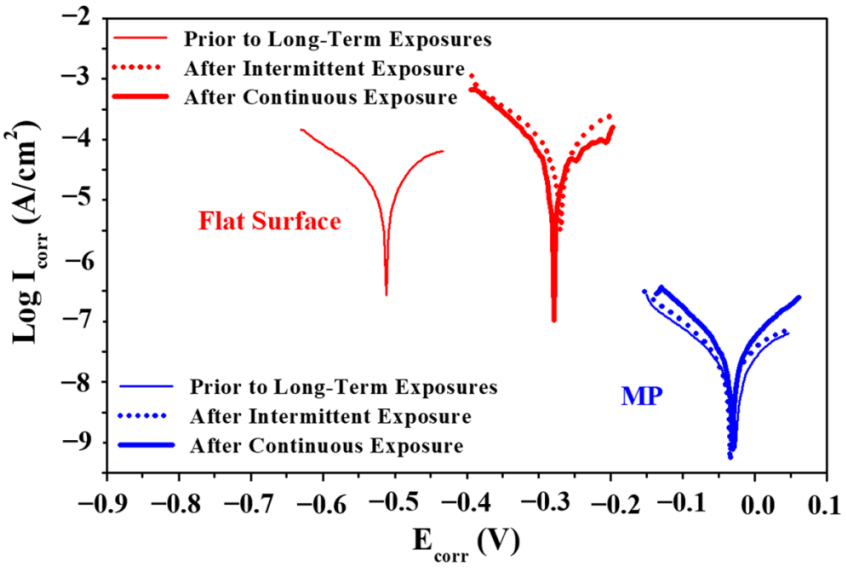

Figure 5. Tafel plots of the flat surface [1] and micropillar surface (MP).

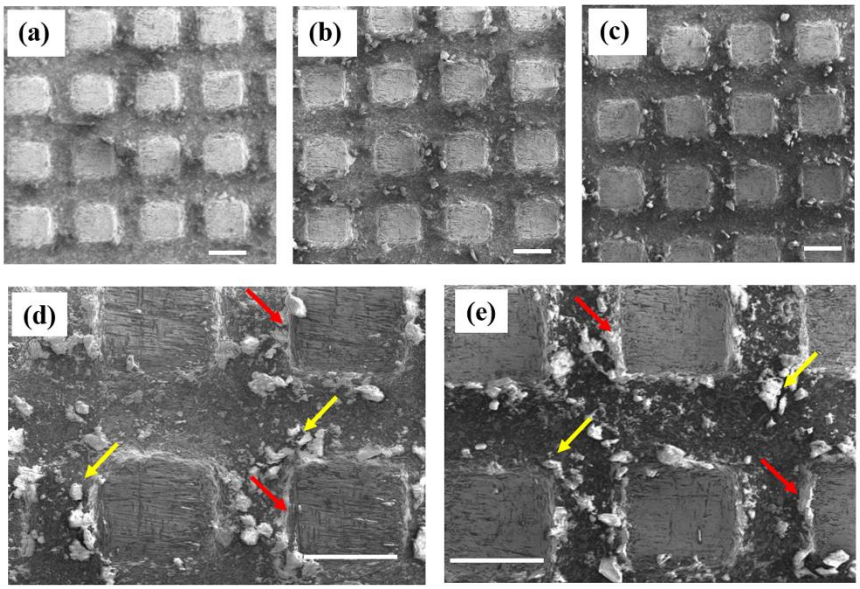

Figure 6. Scanning electron microscopic images of MP surfaces taken after corrosion tests: (**a**) before long-time exposure, (**b**) after intermittent exposure, and (**c**) after continuous exposure to NaCl solution. (**d**,**e**) are high magnification images of (**b**,**c**). Yellow arrows show corrosion products dislodged from the top region of micropillars. Red arrows show wetting of micropillars over their sides adjacent to the top. (Scale bar: 100 μm).

At lower potentials, such as those in the present work, the flat surface shows formation of metastable pits (Figure 7a) [1]. Figure 7b shows metastable pits on the top of a micropillar in MP, after continuous contact with NaCl solution.

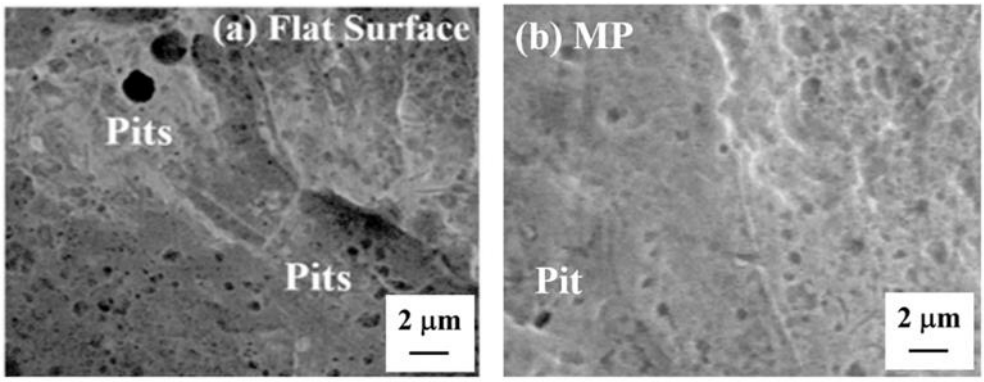

Figure 7. Representative SEM pictures: (**a**) surface of flat sample [1] and (**b**) surface of a micropillar (MP), after corrosion test (upon continuous contact with 3.5 wt.% NaCl solution).

Stainless steels, in their early stage of corrosion, experience damage of passive film by chloride ions, which cause nucleation of metastable pits [24]. Thereupon, re-passivation occurs [24,25]. At potentials higher than the passivation potential, stable pits form which break down passive film [26]. Stable pits are larger in size than metastable pits. For example, stable pits of 50 μm diameter have been observed on 304 L austenitic steel upon contact with 3.5% NaCl [27]. It has been reported that the potential for pitting, above which formation of stable pits occur (E_{pit}), is higher for micropatterns when compared to their flat surfaces [5,8].

Using Equation (4), the efficiency of corrosion inhibition (η, %) of MP was estimated [1,28].

$$\eta = [[i_{corr}\ (flat) - i_{corr}\ (MP)]/i_{corr}\ (flat)] \times 100 \quad (4)$$

η (%) of MP prior to and after long-time contacts with NaCl solution are given in Table 4. MP effectively inhibits saline water corrosion with η values ≥ 77%.

Table 4. Corrosion inhibition efficiency (η) of micropillar surface (MP) prior to and after long-time contacts with NaCl solution, estimated using Equation (4).

Surface	Efficiency of Corrosion Inhibition (η), %		
	BeforeLong-Time Contacts	After Intermittent Contact	After Continuous Contact
MP	88	84	77

The corrosion of SS304 in saline water is severe because of its high surface wettability. By changing the nature of wetting of the steel surface from hydrophilic to composite wetting via topographical modification in the form of micropillars, its corrosion can be readily reduced. An increase in the contact angle or hydrophobicity of micropatterns depends on the (i) dimension of geometrical parameters of their surface features and (ii) the roughness on top of their surface features, as is briefly mentioned in Table 5.

Table 5. Dependence of hydrophobicity on (i) dimension of geometrical parameters of surface features of micropatterns (i.e., micropillar or ridge of microgrooves) and (ii) roughness on top of their surface features. Increase in hydrophobicity of micropatterns decreases liquid mediated corrosion.

Parameter	Hydrophobicity	Ref.
Width	increase in width increases contact area, i.e., solid fraction, and decreases hydrophobicity	[1,9]
Inter-pillar gap or Inter-ridge gap	increase in gap decreases contact area, i.e., solid fraction, and increases hydrophobicity. This occurs until a certain increased value, beyond which, water droplets penetrate the gap between surface features	[5,9]
Height	increase in height often demonstrates increase in water contact angle and increases hydrophobicity	[1,29]
Roughness	increase in roughness decreases contact area and increases hydrophobicity	[1,30,31]

4. Conclusions

In this investigation, an SS304 surface was topographically-modified in the form of micropillars. The micropillar surface was examined for its antiwetting and anticorrosion abilities for long-time duration. The conclusions drawn from the work are:

- SS304 flat surface is hydrophilic in nature, i.e., high surface wettability, due to which its surface gets severely affected by salt-water corrosion.
- The micropillar surface, due to predominant composite wetting, has long-term anti-wetting ability because of the presence of solid-liquid-air interface.
- The antiwetting ability of micropillar surface imparted long-term anticorrosion ability to the steel surface. The micropillar surface significantly lowered corrosion against saline water when compared to the flat surface, due to its smaller area of contact with the corrosive fluid.
- The micropillar surface can provide high efficiency of corrosion inhibition against saline water ($\eta \geq 77\%$) over long-time duration, when exposed intermittently and continuously to NaCl solution.

Topographical modification of SS304 surface in the form of micropillars has immense potential in mitigating liquid-mediated corrosion over a long time duration.

Author Contributions: Conceptualization, V.A.A. and R.A.S.; methodology, V.A.A. and R.A.S.; software, V.A.A., R.A.S., S.J., Y.Z., M.A.K., K.S.R. and R.S.; formal analysis, V.A.A., R.A.S. and S.J.; investigation, V.A.A. and R.A.S.; resources, V.A.A., R.A.S., S.J., Y.Z., M.A.K., K.S.R. and R.S.; data curation, V.A.A., R.A.S., S.J. and K.S.R.; writing—original draft preparation, R.A.S.; writing—review and editing, R.A.S. and S.J.; visualization, V.A.A., R.A.S., S.J., Y.Z., M.A.K., K.S.R. and R.S.; supervision, R.A.S.; project administration, V.A.A., R.A.S. and K.S.R. All authors have read and agreed to the published version of the manuscript.

Funding: This research received no external funding.

Institutional Review Board Statement: Not applicable.

Informed Consent Statement: Not applicable.

Data Availability Statement: Data is contained within the article.

Conflicts of Interest: The authors declare that they have no known competing financial interests or personal relationships that could have appeared to influence the work reported in this paper.

References

1. Annakodi, V.A.; Singh, R.A.; Jayalakshmi, S.; Zhang, Y.; Rao, K.S.; Shabadi, R. Anticorrosion Behaviour of SS304 Microgroove Surfaces in Saline Water. *Metals* **2021**, *11*, 1543. [CrossRef]
2. Lin, N.; Li, D.; Zou, J.; Xie, R.; Wang, Z.; Tang, B. Surface Texture-Based Surface Treatments on Ti6Al4V Titanium Alloys for Tribological and Biological Applications: A Mini Review. *Materials* **2018**, *11*, 487. [CrossRef] [PubMed]
3. Singh, R.A.; Kim, H.J.; Kim, J.; Yang, S.; Jeong, H.E.; Suh, K.Y.; Yoon, E.-S. A biomimetic approach for effective reduction in micro-scale friction by direct replication of topography of natural water-repellent surfaces. *J. Mech. Sci. Technol.* **2007**, *21*, 624–629. [CrossRef]
4. Singh, R.A.; Siyuan, L.; Satyanarayana, N.; Kustandi, T.; Sinha, S.K. Bio-inspired polymeric patterns with enhanced wear durability for microsystem applications. *Mater. Sci. Eng. C* **2011**, *31*, 1577–1583. [CrossRef]
5. de Lara, L.R.; Jagdheesh, R.; Ocaña, J. Corrosion resistance of laser patterned ultrahydrophobic aluminium surface. *Mater. Lett.* **2016**, *184*, 100–103. [CrossRef]
6. Toloei, A.; Stoilov, V.; Northwood, D. A new approach to combating corrosion of metallic materials. *Appl. Surf. Sci.* **2013**, *284*, 242–247. [CrossRef]
7. Guo, M.; Toloei, A.; Rotermund, H.H. The Effect of Surface Patterning on Corrosion Resistance of Biomedical Devices. *J. Mater. Eng. Perform.* **2016**, *25*, 4190–4198. [CrossRef]
8. Trdan, U.; Hočevar, M.; Gregorčič, P. Transition from superhydrophilic to superhydrophobic state of laser textured stainless steel surface and its effect on corrosion resistance. *Corros. Sci.* **2017**, *123*, 21–26. [CrossRef]
9. Anand, A.V.; Arumugam, V.; Jayalakshmi, S.; Singh, R.A. Innovative approach for suppressing corrosion of SS304 steel in saline water environment. *Anti-Corros. Methods Mater.* **2018**, *65*, 484–491.
10. Lian, Z.; Xu, J.; Yu, Z.; Yu, P.; Yu, H. A simple two-step approach for the fabrication of bio-inspired superhydrophobic and anisotropic wetting surfaces having corrosion resistance. *J. Alloy. Compd.* **2019**, *793*, 326–335. [CrossRef]
11. Vaezi, M.; Drescher, P.; Seitz, H. Beamless Metal Additive Manufacturing. *Materials* **2020**, *13*, 922. [CrossRef] [PubMed]
12. World Stainless. Available online: https://www.worldstainless.org (accessed on 7 May 2022).
13. Kim, J.; Sim, S.O.; Park, H.W. Fabrication of durable hydrophobic micropatterns on stainless steel using a hybrid irradiation process. *Surf. Coatings Technol.* **2016**, *302*, 535–542. [CrossRef]
14. Morales, D.M.; Cecilia, C.A. Determination of the corrosion resistance of SS-304 in synthetic seawater at two temperatures using electrochemical noise and polarization curves. *Int. J. Electrochem. Sci.* **2016**, *11*, 8683–8696. [CrossRef]
15. Revie, R.W.; Uhlig, H.H. *Corrosion and Corrosion Control*; John Wiley & Sons: Hoboken, NJ, USA, 2008.
16. Bhushan, B.; Jung, Y.C.; Koch, K. Self-Cleaning Efficiency of Artificial Superhydrophobic Surfaces. *Langmuir* **2009**, *25*, 3240–3248. [CrossRef]
17. Law, K.Y.; Zhao, H. *Surface Wetting*; Springer International Publishing: Cham, Switzerland, 2016.
18. Vrancken, N.; Li, J.; Sergeant, S.; Vereecke, G.; Doumen, G.; Holsteyns, F.; Chen, C.; Terryn, H.; De Gendt, S.; Xu, X. In-situ ATR-FTIR for dynamic analysis of superhydrophobic breakdown on nanostructured silicon surfaces. *Sci. Rep.* **2018**, *8*, 11637. [CrossRef] [PubMed]
19. Fernández, A.; Francone, A.; Thamdrup, L.H.E.; Johansson, A.; Bilenberg, B.; Nielsen, T.; Guttmann, M.; Torres, C.M.S.; Kehagias, N. Hierarchical surfaces for enhanced self-cleaning applications. *J. Micromech. Microeng.* **2017**, *27*, 045020. [CrossRef]
20. Cansoy, C.E.; Erbil, H.Y.; Akar, O.; Akin, T. Effect of pattern size and geometry on the use of Cassie–Baxter equation for superhydrophobic surfaces. *Colloids Surf. A Physicochem. Eng. Asp.* **2011**, *386*, 116–124. [CrossRef]
21. Bormashenko, E. Wetting transitions on biomimetic surfaces. *Philos. Trans. R. Soc. A* **2010**, *368*, 4695–4711. [CrossRef]
22. Bhushan, B.; Jung, Y.C.; Nosonovsky, M. Lotus Effect: Surfaces with Roughness-Induced Superhydrophobicity, Self-Cleaning, and Low Adhesion. In *Springer Handbook of Nanotechnology*; Springer: Berlin/Heidelberg, Germany, 2010; pp. 1437–1524.
23. Herminghaus, S. Roughness-induced non-wetting. *Europhys. Lett.* **2000**, *52*, 165–170. [CrossRef]
24. Loto, R.T. Pitting corrosion resistance and inhibition of lean austenitic stainless steel alloys, Chapter 8. In *Austenitic Stainless Steels—New Aspects*; IntechOpen: London, UK, 2017; pp. 147–170.
25. Tang, Y.; Zuo, Y.; Wang, J.; Zhao, X.; Niu, B.; Lin, B. The metastable pitting potential and its relation to the pitting potential for four materials in chloride solutions. *Corros. Sci.* **2014**, *80*, 111–119. [CrossRef]
26. Fallleiros, N.A.; Wolynec, S. Correlation between corrosion potential and pitting potential for AISI 304L austenitic stainless steel in 3.5% NaCl aqueous solution. *Mater. Res.* **2002**, *5*, 77–84. [CrossRef]
27. Asaduzzaman, M.; Mustafa, C.M.; Islam, M. Effects of concentration of sodium chloride on the pitting corrosion behaviour of AISI-304L austenitic stainless steel. *Chem. Ind. Chem. Eng. Q.* **2011**, *17*, 477–483. [CrossRef]
28. Tong, W.; Karthik, N.; Li, J.; Wang, N.; Xiong, D. Superhydrophobic Surface with Stepwise Multilayered Micro- and Nanostructure and an Investigation of Its Corrosion Resistance. *Langmuir* **2019**, *35*, 15078–15085. [CrossRef] [PubMed]

29. Bae, W.G.; Kim, D.; Song, K.Y.; Jeong, H.E.; Chu, C.N. Engineering stainless steel surface via wire electrical discharge ma-chining for controlling the wettability. *Surf. Coat. Technol.* **2015**, *275*, 316–323. [CrossRef]
30. Guo, P.; Lu, Y.; Ehmann, K.F.; Cao, J. Generation of hierarchical micro-structures for anisotropic wetting by elliptical vibration cutting. *CIRP Ann.* **2014**, *63*, 553–556. [CrossRef]
31. Huerta-Murillo, D.; García-Giron, A.; Romano, J.M.; Cardoso, J.T.; Cordovilla, F.; Walker, M.; Dimov, S.S.; Ocana, J.L. Wetta-bility modification of laser-fabricated hierarchical surface structures in Ti-6Al-4V titanium alloy. *Appl. Surf. Sci.* **2019**, *463*, 838–846. [CrossRef]